Dido disruption leads to centrosome amplification and mitotic checkpoint defects compromising chromosome stability

Varvara Trachana*, Karel H. M. van Wely, Astrid Alonso Guerrero, Agnes Fütterer, and Carlos Martínez-A

Department of Immunology and Oncology, Centro Nacional de Biotecnología/Consejo Superior de Investigaciones Cientificas, Darwin 3, Campus de Cantoblanco, E-28049 Madrid, Spain

Communicated by Antonio Garcia-Bellido, Autonomous University of Madrid, Madrid, Spain, December 18, 2006 (received for review July 17, 2006)

Numerical and/or structural centrosome abnormalities have been correlated with most solid tumors and hematological malignancies. Tumorigenesis also is linked to defects in the mitotic or spindle assembly checkpoint, a key control mechanism that ensures accurate segregation of chromosomes during mitosis. We have reported that targeted disruption of the *Dido* gene causes a transplantable myelodysplastic/myeloproliferative disease in mice. Here, we report that Dido3, the largest splice variant of the *Dido* gene, is a centrosome-associated protein whose disruption leads to supernumerary centrosomes, failure to maintain cellular mitotic arrest, and early degradation of the mitotic checkpoint protein BubR1. These aberrations result in enhanced aneuploidy in the *Dido* mutant cells. *Dido* gene malfunction thus is reported to be part of an impaired signaling cascade that results in a defective mitotic checkpoint, leading to chromosome instability.

aneuploidy | cell cycle | genomic stability

Growing evidence indicates that centrosomes, the microtubule-organizing centers, also serve as scaffolds for many regulatory proteins (1). Because several of these proteins, permanently or transiently associated to centrosomes, are key elements in cell cycle progression (1), centrosome regulation of the cell cycle is the objective of intense study. Centrosomes are comprised of two barrel-shaped centrioles surrounded by an electron-dense matrix of protein aggregates termed the pericentriolar material (PCM). The PCM harbors γ-tubulin ring complexes essential for microtubule nucleation (2). The centrosome duplicates during the S phase to yield two centrosomes that instruct formation of the bipolar spindle. Formation and correct positioning of a bipolar mitotic spindle is essential for correct chromosome congression and subsequent segregation (3). Elimination of the regulatory mechanisms that govern centrosome duplication result in more than two centrosomes (centrosome amplification), which could lead to aberrant mitoses and chromosome segregation errors (4).

Correct chromosome segregation is regulated by a mechanism known as the mitotic or spindle-assembly checkpoint (SAC), which monitors microtubule attachment to chromosome kinetochores (5). Stable bipolar attachment of kinetochores to microtubules leads to dissociation of kinetochore-associated Bub and Mad family proteins (6). If a kinetochore is not connected to microtubules and/or tension is not created, SAC proteins emit a "wait anaphase" signal that diffuses to the cytoplasm. This signal is thought to consist of Bub3, BubR1, and Mad2 complexes that bind to and inhibit Cdc20; Cdc20 is a coactivator of the anaphase-promoting complex (APC/C), which targets substrates for degradation by the proteosome (7). Correct alignment of all mitotic chromosomes at the metaphase plate inactivates the SAC, activating the APC/C and triggering destruction of cyclin B1 and other mitotic regulators; this drives metaphase-to-anaphase transition (8).

Defects in the mitotic checkpoint contribute to the chromosome instability observed in cancer (9). Although SAC impairment is frequent in many cancers, relatively few genetic alterations in SAC proteins have been found in tumors (10, 11), suggesting that chromosome instability in cancer may be due to altered epigenetic control of SAC components at the protein level (12). Complete inactivation of the SAC genes results in rapid death in vertebrates (13), whereas cells and organisms with a weakened checkpoint survive and develop chromosome instability (14). A weakened checkpoint could result from heterozygous loss of SAC genes (15, 16) or disruption of other yet-unidentified genes responsible for SAC protein stabilization (12).

Cells with a dysfunctional SAC and consequent chromosome missegregation often fail to complete cytokinesis (17). Premature or mislocated cytokinesis can result in breakage of segregating chromosomes, whereas cytokinesis delay or its bypass could produce binucleated cells, leading to polyploid or aneuploid daughter cells; such events are observed in various cancers (18). Although the causes of binucleation are ill-defined, such defects were described as early markers of preleukemic lesions (19, 20), linking SAC-related defects to hematological malignancy.

The death inducer-obliterator (*Dido*) gene is implicated in the induction of hematological myeloid neoplasms. Through alternative splicing, the *Dido* gene gives rise to three polypeptides (Dido1, Dido2, and Dido3); Dido3 is the dominantly expressed isoform (21). Here, we show that only the Dido3 isoform localizes at the centrosomes of interphase cells and migrates to the spindle poles during mitosis. We demonstrate that targeted disruption of the *Dido* gene gives rise to centrosome amplification, a weakened SAC, and division defects that challenge chromosome stability. We also suggest that Dido3 disruption leads to early degradation of the mitotic checkpoint "master" molecule BubR1 that, in turn, leads to cell exit from mitosis without ensuring equal chromatin segregation. Dido3 is thus a previously undescribed centrosome-associated protein, proposed here to be involved in the mitotic checkpoint signaling cascade, possibly explaining *Dido* gene implication in the induction of cell transformation.

Results

Dido3 Is a Centrosome-Associated Protein. Homozygous or heterozygous disruption of *Dido* by gene targeting causes transplantable myelodysplastic syndrome (MDS)/myeloproliferative disorder (MPD) in mice, whereas all human MDS/MPD patients have altered *Dido* RNA levels (21). Based on domain identification, *Dido* was suggested to contribute to chromosome stability; homozygous *Dido*-targeted murine embryonic fibroblasts (MEFs) (*Dido*-mutant MEFs) have a high incidence of lagging chromosomes (22). Of the three *Dido* isoforms (Dido1, Dido2, and Dido3), the largest (Dido3)

Author contributions: V.T. and C.M.-A. designed research; V.T., K.H.M.v.W., A.A.G., and A.F. performed research; V.T., K.H.M.v.W., A.A.G., A.F., and C.M.-A. analyzed data; and V.T. wrote the paper.

The authors declare no conflict of interest.

Abbreviations: APC/C, anaphase-promoting complex; BM, bone marrow; MDS, myelodysplastic syndrome; MPD, myeloproliferative disorder; MEF, murine embryonic fibroblast; PCM, pericentriolar material; SAC, spindle-assembly checkpoint.

*To whom correspondence should be addressed. E-mail: trachana@cnb.uam.es.

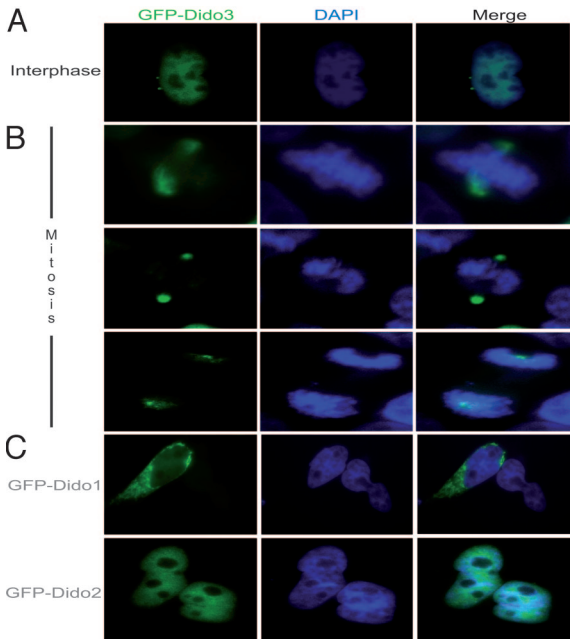

Fig. 1. Dido3 localizes at centrosomes/spindle poles. (*A*) Dido3 has a distinct two-dot localization pattern in HeLa cells, reminiscent of centrosomes (interphase). (*B*) During mitosis, Dido3 translocates to mitotic poles in early metaphase and remains pole-associated throughout mitosis. (*Upper*) Dido3 localization early in mitosis. (*Middle* and *Bottom*) Mid- and late mitosis, respectively. (*C*) GFP-Dido1 is seen mainly in cytoplasm of HeLa cells (*Upper*), whereas GFP-Dido2 is nuclear (*Lower*). These isoforms did not associate with centrosomes or spindle poles.

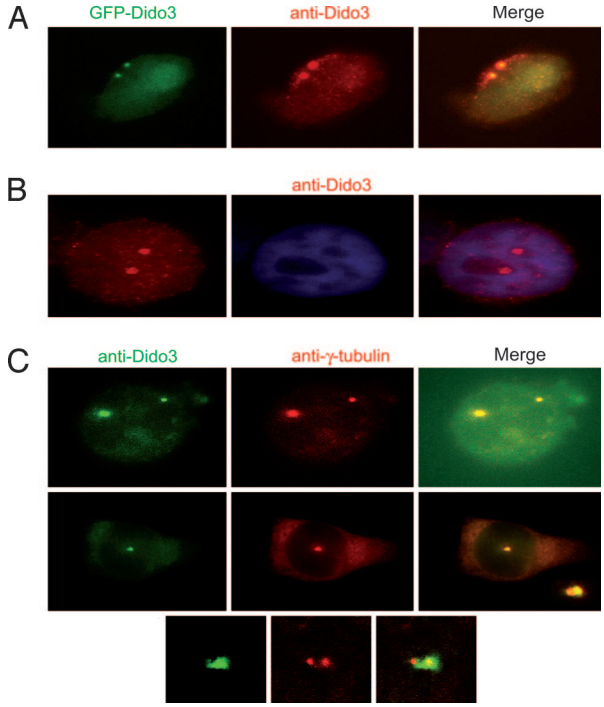

Fig. 2. Endogenous human Dido3 colocalizes with γ-tubulin. (*A*) HeLa cells expressing GFP-Dido3 (green), stained with anti-Dido3 (red), showed overlapping localization. (*B*) In untransfected HeLa cells, anti-Dido3 (red) revealed the same pattern for endogenous human Dido3 as for GFP-Dido3. (*C*) Staining of HeLa cells with anti-Dido3 (green) and anti-γ-tubulin (red) confirmed Dido3 centrosome localization. Confocal microscopy images of Dido3 (green) and γ-tubulin (red) localization indicated possible differences in the amount of Dido3 associated with each centrosome when centrosomes were in proximity (*Middle* and *Bottom*).

is dominantly expressed in most human and mouse cell lines and tissues. Moreover, MEFs express only Dido3 in detectable amounts (21). Because these observations imply a cell cycle-related role for Dido3, we examined its subcellular localization to further analyze its function.

We studied murine Dido3 (mDido3) localization by detecting GFP-tagged fusion protein in HeLa cells. In interphase HeLa cells, Dido3 localized to the nucleus, but we also distinguished a two-dot pattern near the nucleus, reminiscent of centrosomes (Fig. 1*A*). Early in mitosis, Dido3 began to concentrate at the spindle poles (Fig. 1*B Top*); maximum concentration at poles was reached later in mitosis (Fig. 1*B Middle* and *Lower*). Dido1 and Dido2 showed distinct localization patterns; Dido2 was found in the nucleus, whereas Dido1 was mainly cytoplasmic. Neither isoform associated with centrosomes or cytoskeletal elements (Fig. 1*C*).

Dido3 Colocalizes with γ-Tubulin at Centrosomes. To confirm Dido3 subcellular localization, we used an Ab to a peptide corresponding to the last 20 aa of the mDido3 C-terminal region (anti-Dido3). Anti-Dido3 staining overlapped GFP-mDido3 localization in HeLa cells (Fig. 2*A*). This Ab also showed that endogenous human Dido3 localization in untransfected HeLa cells was indistinguishable from that of GFP-mDido3 (Fig. 2*B*).

To verify Dido3 centrosome association, we double-stained cells with anti-Dido3 and anti-γ-tubulin. Merged images showed Dido3 and γ-tubulin colocalization at the centrosomes (Fig. 2*C*), with a possible difference in Dido3 association to one of the two centrosomes (Fig. 2*C Middle* and *Bottom*). Anti-Dido3 preferentially stained the PCM of one of the two centrosomes early in the centrosomal cycle, as determined by centrosome proximity. When centrosomes were well separated and moved toward the poles, Dido3 staining appeared to be uniform for the two centrosomes (Fig. 2 *B* and *C Upper*). Centrosomes mature during the S-to-M transition; when M phase is reached, both centrosomes have acquired maximum amounts of PCM (23). Differences in Dido3 association might be linked to variations in the PCM accumulated in each centrosome during maturation.

***Dido* Disruption Leads to Centrosome Amplification.** Targeted disruption of the *Dido* gene (Fig. 3*Ai*) results in an N-terminally truncated Dido3 form, Dido3ΔNT (21) (Fig. 3*Aii*). In Western blot analysis of WT and *Dido*-mutant primary MEF lysates, anti-Dido3 also recognized Dido3ΔNT because of its intact C-terminal domain (Fig. 3*Aiii*). As MEFs express only Dido3, any differences in *Dido*-mutant MEFs could be attributed to only Dido3 disruption and not to Dido1 or Dido2. To determine whether Dido3 truncation alters its localization, we stained WT and mutant MEFs with anti-Dido3. Whereas in WT MEFs, Dido3 localized at centrosomes/spindle poles (Fig. 3*B i* and *ii*), in mutant cells, Dido3ΔNT lost clear centrosome association (Fig. 3*B iii* and *iv*). Mitotic mutant cells, in which truncated Dido3 protein failed to migrate to the poles (Fig. 3*Biv*), showed defects in chromosome alignment in the metaphase plate.

To evaluate possible *Dido* disruption-induced centrosome changes, we stained mutant cells with anti-γ-tubulin and anti-centrin, because centrin is a centriole and PCM component (24). Mutant cells showed centrosome amplification, frequently with three to six centrosomes per cell; 12 or more centrosomes were found in some cases (Fig. 4*Ai*). Anti-centrin staining confirmed centrosome amplification (Fig. 4*Aii*). Staining with anti-α-tubulin showed that abnormal centrosome number often resulted in spindle malformation (Fig. 4*Aiii*). Analysis of centrosome number per cell showed that the number of mutant cells with more than two centrosomes was significantly higher compared with WT cells (Fig. 4*Bi*).

Because the *Dido* gene is implicated in induction of MDS/MPD,

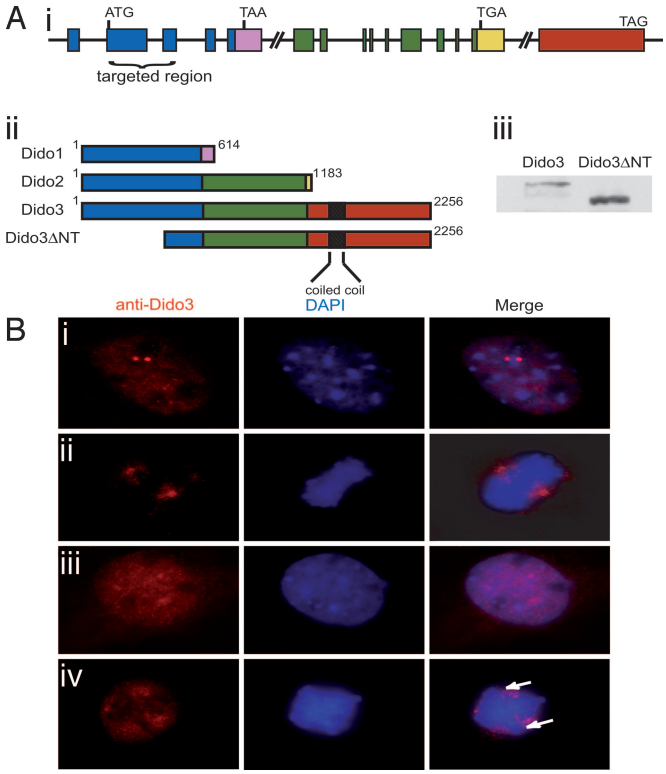

Fig. 3. Targeted *Dido* gene disruption results in an N-terminal-truncated Dido3 form that loses centrosome association. (*Ai*) *Dido* gene architecture. A common N-terminal domain (blue) is followed by a specific C-terminal domain for each of the three splice variants (pink, green, yellow, and red). The domain targeted in mutant mice is indicated. (*Aii*) Dido3ΔNT is the truncated Dido3 form in mutant cells after disrupting the targeted region of the *Dido* gene, as in *Ai*. (*Aiii*) Western blot of WT and *Dido*-targeted (mutant) MEF lysates stained with anti-Dido3. The lower band is the truncated form of Dido3. (*B*) MEFs were stained with anti-Dido3 (red) and DAPI (blue). (*Bi* and *Bii*) In interphase (*Bi*) and mitotic (*Bii*) WT cells, Dido3 clearly associates with centrosomes/spindle poles. (*Biii*) In interphase mutant cells, the Dido3-truncated form shows a diffuse nuclear localization without the two-dot centrosome pattern. (*Biv*) In mitotic mutant cells, there is no spindle pole association and chromosomes appear to be misaligned (arrows).

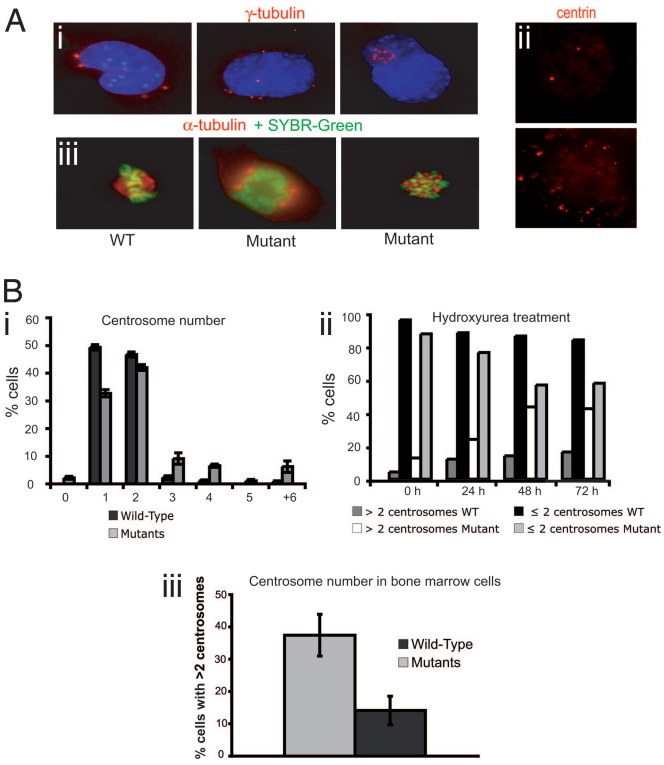

Fig. 4. Targeted *Dido* disruption leads to centrosome amplification and spindle malformation. (*Ai*) Anti-γ-tubulin staining revealed mutant MEFs with 4, 8, or 12 centrosomes. (*Aii*) Anti-centrin staining confirmed centrosome amplification in mutant cells (*Lower*), whereas WT MEFs showed normal numbers (*Upper*). (*Aiii*) MEFs were stained with anti-α-tubulin (red) to show spindle formation. DNA was stained with SYBR-Green. WT MEFs (*Left*) had normal spindle formation. Mutants formed a spindle with four poles (*Center*) or a completely disorganized spindle (*Right*). (*Bi*) We counted centrosomes in anti-γ-tubulin-stained WT and mutant MEFs. The *x* axis shows centrosomes per cell. Approximately 23% of *Dido*-mutant cells had three or more centrosomes, whereas only 3.9% of WT cells showed this abnormal number. (*Bii*) Percentage of WT and mutant MEFs showing ≤2 or >2 centrosomes per cell after hydroxyurea treatment. The percentage of mutant cells with aberrant centrosome numbers increased with time, reaching >40% of total cells at 48 h. The *x* axis depicts time of hydroxyurea treatment. (*Biii*) Freshly isolated BM samples stained with anti-γ-tubulin. A significantly larger percentage of cells from mutant mice had more than two centrosomes compared with cells from WT mice (Student's *t* test, $P = 0.008$).

we analyzed hematopoietic cells from bone marrow (BM) for alterations in centrosome number. Staining of WT and mutant BM cells with γ-tubulin showed a significantly larger number of cells with centrosome amplification in targeted mice (Fig. 4*Biii*). The mice (WT and mutant) included in this experiment were 9 months of age or older. Mutant mice younger than 3 months old showed no clear alterations in centrosome number of BM cells. Because MDS/MPD onset was detected at ≈7 to 8 months of age (21), these findings strengthen a possible correlation between disease development and the centrosome aberrations in BM cells.

The centrosome duplication mechanism is under tight control of a checkpoint that ensures that the centrosome duplicates only once per cycle, during S phase (3). When cells are arrested in S phase with DNA replication-blocking drugs such as hydroxyurea, only a single centrosome duplication round can occur. If the duplication mechanism is impaired, hydroxyurea treatment leads to multiple duplication rounds, resulting in supernumerary centrosomes (25). To determine whether *Dido* is involved in centrosome duplication, we treated WT and mutant MEFs with hydroxyurea, harvested cells at various times, and stained with γ-tubulin. The number of mutant MEFs with elevated centrosome number increased with time (>40% of mutants had supernumerary centrosomes at 72 h after treatment (Fig. 4*Bii*). The aberrations in centrosome number in mutant MEF and BM cells, as well as the elevated centrosome number after hydroxyurea treatment, suggest that *Dido* is implicated in regulating centrosome duplication.

***Dido* Gene Targeting Leads to SAC Impairment.** Supernumerary centrosomes can lead to aberrant mitoses and chromosome missegregation (4). Because chromosome segregation is under the control of the SAC, we tested its function in *Dido*-mutant cells. The dynamic balance between spindle microtubule polymerization/depolymerization is critical for cell entry and exit from mitosis. Drugs that disrupt these dynamics, such as taxol and nocodazole, trigger the SAC, leading to cell arrest in mitosis (26). To study Dido3 involvement in SAC, we treated WT and mutant cells with taxol and nocodazole and determined the mitotic population by propidium iodide staining. In the presence of the spindle toxins, mutant MEFs did not maintain mitotic arrest for longer than 16–18 h, giving rise to an additional 2N population (Fig. 5*A*), whereas WT cells continued in arrest for at least 30 h (data not shown). Mutant MEFs thus easily overcame mitotic arrest after spindle disruption, indicative of a dysfunctional SAC.

For metaphase-to-anaphase progression, the SAC must be switched off, which signals APC/C-mediated degradation. Cyclin

CELL BIOLOGY

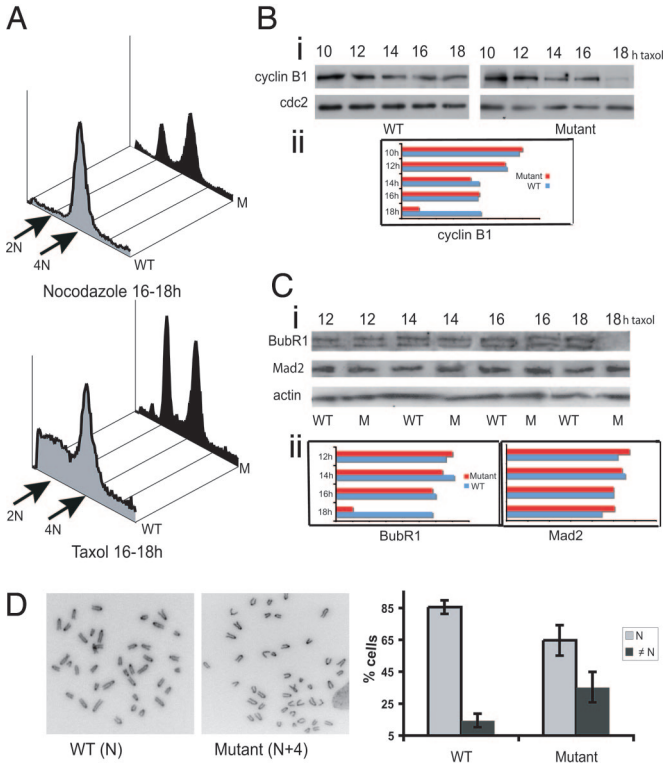

Fig. 5. *Dido* disruption leads to a dysfunctional SAC and enhanced chromosome instability. (*A*) WT and mutant cells were presynchronized with aphidicolin and released into nocodazole (*Upper*) or taxol (*Lower*) to trigger mitotic arrest. Cells were fixed, propidium iodide-stained, and analyzed by FACS. The majority of WT cells were arrested as a 4N population, whereas mutant cells failed to maintain arrest for longer than 16–18 h, giving rise to an additional 2N population. The figure is representative of at least four independent experiments of drug treatment for 16–18 h. (*Bi*) WT and mutant cells, taxol-treated as above for the times indicated, were tested in Western blot with equal amounts of total cell lysates by using anti-cyclin B1 (*Upper*). Coincident with the rapid decrease in the mitotic population of mutant cells at 16–18 h after taxol treatment (*A*), cyclin B1 levels dropped drastically after 16 h. cdc2 protein levels were unchanged in both cell types (*Lower*). (*Bii*) Quantification of cyclin B1 levels from WT and mutant cell lysates. Quantification was performed on the Western blots by using ImageJ software. (*Ci*) Cell lysates as in *B* were tested in Western blot with anti-BubR1 (*Top*). The double band probably represents hyper- and hypophosphorylated BubR1 forms. At 16 h after taxol treatment, BubR1 levels were no longer detected in mutant cells. Mad2 protein levels were unchanged and were similar for WT and mutant cells (*Center*). Anti-actin was used as loading control (*Bottom*). (*Cii*) Quantification of BubR1 (*Left*) and Mad2 levels (*Right*), as in *Ci*. (*D Left* and *Center*) Metaphase spreads from WT (*Left*) and mutant (*Center*) MEFs treated with colcemid for 4 h. (*Right*) Individual chromosome counts from WT (left) and mutant (right) MEFs were grouped as cells with normal karyotype (diploid, N) and cells with abnormal karyotype (aneuploid, ≠N). The percentage of aneuploid mutant cells was significantly higher than that of WT cells (Student's *t* test, $P = 0.0088$).

B1 destruction marks this cell transition; we thus analyzed cyclin B1 levels to confirm that mutant cells exited arrest in the presence of spindle-disrupting drugs. As predicted, cyclin B1 levels in mutant MEFs were reduced greatly after 16 h taxol treatment (Fig. 5*B*), coinciding with a rapid decrease in the mitotic population (Fig. 5*A*). In these conditions, cyclin B1 levels in WT cells remained high, because the majority of WT MEFs were arrested as a mitotic 4N population. cdc2 protein kinase levels also remained high in both cell types (Fig. 5*B*), indicating that cyclin B1 destruction is specific, probably due to SAC signaling errors.

During mitotic arrest in metaphase, SAC inhibition of APC/C-mediated proteolysis involves BubR1, Bub3, Mad2, and cdc20 protein complexes (7). To explain the inefficient SAC signaling in *Dido*-mutant cells, which results in early slippage from mitotic arrest, we analyzed BubR1 and Mad2 levels after taxol treatment. BubR1 was undetectable in mutant MEFs after 16-h treatment, similar to cyclin B1 and concurring with the drop in the mitotic population; BubR1 levels were unchanged in WT cells, as were Mad2 levels in both cell types (Fig. 5*C*). BubR1 is significantly reduced in ≈30% of human adenocarcinomas and also is degraded after prolonged spindle damage (12). The striking early BubR1 decrease in *Dido* mutant cells could be due to accelerated degradation and consequent premature APC/C activation, leading to premature metaphase exit.

A malfunctional SAC, which leads to premature cell exit from metaphase before all chromosomes align at the metaphase plate, compromises chromosome stability (9). Instability in *Dido* mutant cells was suggested by increased numbers of lagging chromosomes (22) as well as by an elevated micronucleus formation rate compared with WT cells (data not shown). Chromosome counts on metaphase spreads confirmed enhanced chromosome instability due to *Dido* disruption (Fig. 5*D*). Mutant MEFs showed a significant increase in the frequency of aneuploidy (≠N) compared with WT MEFs, which have a fairly stable diploid karyotype (N). More than 50% of the mutant aneuploid cells had $n \pm 1$ to $n \pm 4$ chromosomes. These observations strongly suggest a compromised SAC.

Cytokinesis Defects in *Dido*-Mutant Cells. Chromosome misalignment could lead to cytokinesis failure (17), which is characterized by intercellular cytoplasmic bridges and binucleated cells (18). As chromosome segregation appears to be challenged in *Dido*-mutant cells, probably due to SAC defects, we studied the mitotic exit of these cells. We stained mutant MEFs with anti-γ-tubulin and examined them for anomalies. A large percentage of targeted cells remained connected by intercellular bridges or aborted cytokinesis to form binucleated cells (Fig. 6*A i* and *ii*). We used a specific cytoplasmic membrane probe to confirm binucleated cells by confocal microscopy. Adjacent cells that had divided normally showed clear membrane staining between nuclei, whereas nuclei were enclosed within a single membrane in mutant binucleated cells (Fig. 6*Aiii*). A significantly larger number of mutant MEFs had cytokinesis defects compared with WT cells (Fig. 6*B*).

We also observed cytokinesis defects in BM cells of *Dido*-targeted mice. Freshly isolated BM had a large proportion of binucleated cells, which increased after 6 days in culture (Fig. 6*Aiv*). These data further indicate Dido3 involvement in cytokinesis and specifically link *Dido* disruption to formation of binucleated cells, a common dysplastic feature (19, 20).

Discussion

Partial or complete loss of *Dido* function is found in all MDS/MPD patients and in most other patients with myeloid malignancies; *Dido*-mutant mice, generated by gene targeting, suffer a similar disease (21). Homozygous *Dido*-disrupted MEFs, which normally express only Dido3, show increased frequency of anaphase-lagging chromosomes (22). We demonstrate here that Dido3 is a centrosome/spindle pole-associated protein and that the *Dido*-disruption results in an N-terminal-truncated Dido3 isoform that loses its centrosomal association. *Dido*-mutant cells have supernumerary centrosomes and high incidence of cytokinesis errors, resulting in enhanced chromosome instability. Mutant cells override induced mitotic arrest with synchronous degradation of the checkpoint molecule BubR1. We speculate that the lack of the Dido N terminus-specific domain disturbs its localization, resulting in functional aberrations. Intact, fully functional Dido3 that localizes on interphase centrosomes and concentrates on spindle poles during mitosis thus may be part of the signaling network responsible for centrosome-mediated regulation of mitotic transitions and checkpoint signaling.

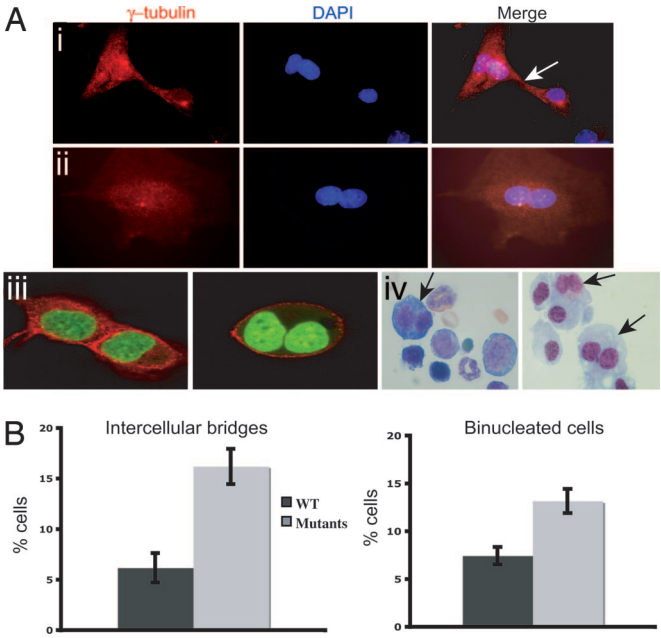

Fig. 6. *Dido* mutants have cytokinesis defects. (*A*) *Dido*-mutant MEFs were stained with anti-γ-tubulin (red) and DAPI (blue). (*Ai*) Cells connected by an intercellular bridge (arrow). (*Aii*) A typical double-nucleus phenotype, indicating cell division failure. (*Aiii*) To confirm the existence of binucleated cells, we used a cytoplasmic membrane probe in confocal microscopy; DNA was stained with SYBR-Green. Two adjacent but separate WT cells are seen (*Left*). Binucleated mutant cells show a single membrane around the nuclei (*Right*). (*Aiv*) Representative images of bone marrow samples from *Dido*-targeted mice; arrows indicate binucleated cells in freshly isolated (*Left*) or 6-day cultured BM cells (*Right*). (*B*) Quantification of defective divisions. A significantly larger percentage of *Dido*-mutant than WT cells remained joined by intercellular bridges (Student's *t* test, $P = 0.0015$). A larger percentage of mutant than WT cells were binucleated (Student's *t* test, $P = 0.0031$).

In a comprehensive proteomic analysis of human interphase centrosomes, Andersen *et al.* (27) identified the majority of known centrosomal proteins and 23 novel components and 41 likely candidates. Dido3 was not on these lists. As the authors of this work pointed out, however, their approach also was unable to identify some known structural centrosomal proteins, as well as one-third of the regulatory proteins known to localize on the centrosome in interphase. It should be mentioned that Dido3 is found on interphase centrosomes but is more abundant on the mitotic spindle poles; Andersen *et al.* (27) stated that although they consider their approach highly successful, it has limitations in revealing variations in centrosome composition during the cell cycle.

Centrosome amplification is common in many types of malignancy (4). Numerical and structural centrosome abnormalities are reported in acute myeloid malignancy (28) and are common in MDS and aplastic anemia (29), as well as in chronic myelogenous leukemia, a typical MPD (30). We show that disruption of centrosome-associated Dido3 gives rise to multiple centrosomes in a significant percentage of MEF and BM cells. Amplification of centrosome number after hydroxyurea treatment suggests *Dido* involvement in the centrosome duplication mechanism.

The mitotic checkpoint or SAC ensures correct chromosome segregation, because it inhibits anaphase onset until all kinetochores are attached to the spindle and tension is generated (5). The SAC initially was recognized 15 years ago by using spindle-disrupting drugs (31); testing cell ability to arrest in response to microtubule poisons has since become a common test of checkpoint competence. We observed that *Dido*-mutant cells failed to maintain arrest in the presence of spindle toxins and exited metaphase with a parallel decrease in cyclin B1, indicating inefficient APC/C inhibition probably due to SAC signaling errors.

After prolonged mitotic arrest due to spindle damage, even cells without known mitotic checkpoint defects eventually slip mitotic arrest and exit mitosis in a process termed adaptation (32). In human cells, adaptation is concomitant with gradual BubR1 degradation and a subsequent increase in polyploidy. BubR1 degradation is specific, with no apparent changes in other kinetochore proteins; its instability thus might be implicated in generation of polyploidy, providing a functional link between BubR1 degradation and carcinogenesis (12). As *Dido*-mutant cells exited metaphase after 16-h exposure to spindle toxins, BubR1 levels dropped substantially. It has been proposed that destabilization of the SAC proteins can be caused by deregulation of other genes and their products (12, 33); to our knowledge, no such genes have yet been identified. We suggest that Dido3, a centrosome-associated protein, could function as part of the fail-safe mechanism responsible for monitoring BubR1 levels. This implies that Dido3, a nonkinetochore-associated protein, is part of the network of regulatory molecules involved in the mitotic checkpoint signaling.

SAC signaling is not entirely absent in *Dido*-mutant cells. Mutant cells are arrested for at least 16 h in the presence of spindle poisons before inappropriate exit. *Dido* mutation thus probably leads to checkpoint weakening, rather than complete inactivation. Complete lack of SAC signaling causes missegregation of large numbers of chromosomes, resulting in immediate cell death, as seen in cells with total inactivation due to siRNA-mediated Mad2 or BubR1 depletion (13). Cells and organisms with a weakened checkpoint remain viable but show increased aneuploidy (34). The usual chromosome number in these aneuploid cells is very close to the diploid number (± 4), with ± 1 being the most common karyotype (14). Such aneuploidy is observed in *Dido* mutant cells, supporting our proposal that the SAC in these cells is weakened rather than completely dysfunctional.

Calculating the mitotic index in response to spindle toxins indicates a cell's ability to sustain extended mitotic arrest, although this may be an inaccurate measure of checkpoint signaling. Demonstrating the failure of cells to maintain mitotic arrest nonetheless provides a triggering link between this defect and malignant evolution (10, 35). Here, we propose that the causes of a weakened SAC, which leads to early escape from arrest, could involve alterations of genes other than the known SAC genes, such as the newly identified *Dido*. The implication of such genes in tumorigenesis would suggest their involvement in SAC signaling.

Supernumerary centrosomes could cause chromosome segregation errors that, in the absence of a robust SAC, might lead to cytokinesis defects (17). *Dido* mutant cells show a high incidence of binucleated cells and intercellular bridges, features highly suggestive of aberrant cytokinesis. Such anomalies are common in mutants of genes responsible for maintaining genomic stability, e.g., mutation or elimination of p53 or p53 downstream effectors such as Gadd45a (36). Cytokinesis failure in these mutants has been demonstrated to result from uncoupling centrosome duplication-DNA replication during S phase (37). The hydroxyurea experiment discussed earlier suggested that these normally tightly associated processes also are affected in Dido3-targeted cells; the anomalies observed here in cytokinesis thus might be the late outcome of S phase deregulation. Alternatively, direct interference with the completion of cell division has been argued for p53-null cells (38), which could also be the case for *Dido* mutants. A more detailed study of S phase in *Dido*-targeted cells is necessary to determine whether either of these possibilities can be excluded.

Several studies connect centrosomes with progression from G_1 to S (39), G_2 to M (40), metaphase to anaphase (41), and cytokinesis (42). Although these findings provide evidence that associate centrosomes with cell cycle checkpoints and mitotic transitions, the molecular interactions underlying specific centrosome protein dysfunction and cell transformation remain an open issue. Here, we

show that disruption of the *Dido* gene, which is implicated in the induction of hematological malignancies, gives rise to centrosome amplification, a malfunctioning SAC and cytokinesis defects, compromising chromosome stability. *Dido* gene mutation thus may be part of the genetic damage to hematopoietic progenitor cells that leads to karyotype destabilization via aberrant mitosis. Our findings on *Dido* function connect specific centrosome protein dysfunction with the mitotic checkpoint weakening that facilitates tumorigenesis.

Materials and Methods

Cell Culture and Synchronization. Cell lines and WT and *Dido*-mutant early passage (p1–p4) primary MEFs were cultured in DMEM with 10% heat-inactivated FBS, glutamine, and antibiotics (37°C with 5% CO_2). We performed morphological analysis of BM samples on May-Grünwald/Giemsa-stained cytospins (10^5 total cells). We cultured BM samples in Iscove's modified Dulbecco's medium with 30% FBS/15% IL-3/10 units/ml erythropoietin/50 ng/ml stem cell factor.

MEFs were synchronized at G_1/S with a 16-h aphidicolin block (10 μg/ml; Sigma, St. Louis, MO). For mitotic arrest, synchronized cells were treated for 18 h with Paclitaxel (taxol, 0.2 μM; Sigma) or nocodazole (0.4 μg/ml; Sigma). To block DNA replication, cells were treated with 2 mM hydroxyurea (Sigma).

Plasmids and Cell Transfection. To generate a GFP-Dido1 fusion protein, the *Dido1* ORF, flanked by BamHI and ApaI sites (43), was cloned into BglII and ApaI sites in the pGFP-C1 vector (BD Clontech, Mountain View, CA). Vectors expressing GFP-Dido2 and -Dido3 fusions were constructed by replacing an internal BglII-NotI fragment with *Dido2*- or *Dido3*-specific parts. Cells were transfected at 50–60% confluence by using plasmid DNA (5 μg) and FuGENE 6 (15 μl; Roche, Basel, Switzerland). Protein expression was permitted for 24–48 h, after which cells were processed for immunofluorescence.

Western Blot, Antibodies, and Reagents. For Western blot analysis, whole-cell lysates were prepared in loading buffer and boiled. After SDS/PAGE, proteins were transferred to PVDF membranes (Bio-Rad, Hercules, CA). Rabbit anti-Dido-3 Ab was raised against a peptide corresponding to the C-terminal final 20 aa of mDido3 and purified by using the immunizing peptide. It specifically recognizes Dido3 in MEF lysates and in immunofluorescence of mouse and human cells; competition with the immunizing peptide blocks the signal (data not shown). We used Ab to cyclin B1 (1:1,000; BD Pharmingen, San Diego, CA), cdc2 (1:200; Santa Cruz, Santa Cruz, CA), BubR1 (1:5,000; Novus, Littleton, CO), Mad2 (1:2,000; Abcam, Cambridge, U.K.), and actin (1:1,000; Sigma), as well as peroxidase-conjugated anti-mouse, -rabbit, or -goat secondary Ab (Roche), followed by chemiluminescent detection reagent (ECL; Roche).

For immunofluorescence, we used Ab to γ-tubulin (1:1,000; Sigma), centrin (1:200; Abcam), and α-tubulin (1:500; Sigma), and rabbit anti-Dido3 (1:100), and Cy2- or Cy3-goat anti-rabbit/mouse secondary Ab (1:200–1:800; The Jackson Laboratory, Bar Harbor, ME).

Cell Cycle Analysis. Cells were washed with cold PBS and fixed with 100% ethanol (4°C for $\geq$1 h). Propidium iodide (Beckman Coulter, Fullerton, CA) was added, followed by incubation (30 min at 37°C in the dark). Stained cells were analyzed in a Coulter EPICS XL cytometer (Beckman Coulter).

Immunofluorescence Microscopy. Cells were washed with PBS, fixed in 100% methanol (10 min), permeabilized with 0.1% Triton X-100 in PBS (Sigma), then blocked with 3% BSA in PBS (10 min at room temperature). All primary Ab were incubated for 1 h at room temperature. Coverslips were mounted by using VECTASHIELD with DAPI (Vector Laboratories, Burlingame, CA) or SYBR-green (Invitrogen, Carlsbad, CA) to visualize DNA. For cytoplasmic membrane staining, cells were loaded with 6 μg/ml fluorescein-conjugated cholera toxin (5 min at room temperature; Sigma).

Immunofluorescence was analyzed on a Leica microscope, and images were taken with an Olympus DP70 camera. Confocal images were captured on a Leica TCS NT laser scanning microscope.

Cytogenetics. MEFs were seeded 24 h before colcemid treatment (0.1 μg/ml, 4 h; Sigma) for metaphase arrest. Cells were detached from plates, incubated in 0.56% KCl (10 min at 37°C), then fixed in three changes of methanol/acetic acid (3:1). Fixed pellets were used for slide spreads. At least 65 DAPI-stained metaphase spreads were examined for WT and mutant MEFs.

We thank M. C. Moreno-Ortiz for help with flow cytometry and C. Mark for editorial support. This work was supported by Spanish Education and Science Ministry Grant GEN2001-4856-C13-01, Health Ministry Grant PI051965, and the Lilly Foundation. K.H.M.v.W. received Grant RyC2004–1886 from the Education and Science Ministry. The Department of Immunology and Oncology was founded and is supported by the Spanish National Research Council and Pfizer.

1. Doxsey S, McCollum D, Theurkauf W (2005) *Annu Rev Cell Dev Biol* 21:411–434.
2. Moritz M, Braunfeld MB, Sedat JW, Alberts B, Agard DA (1995) *Nature* 378:638–640.
3. Rudner AD, Murray AW (1996) *Curr Opin Cell Biol* 8:773–780.
4. Doxsey SJ (2001) *Nat Cell Biol* 3:105–108.
5. Musacchio A, Hardwick KG (2002) *Nat Rev Mol Cell Biol* 3:731–741.
6. Millband DN, Hardwick KG (2002) *Mol Cell Biol* 22:2728–2742.
7. Taylor SS, Scott MI, Holland AJ (2004) *Chromosome Res* 12:599–616.
8. Yu H (2002) *Curr Opin Cell Biol* 14:706–714.
9. Kops GJ, Weaver BA, Cleveland DW (2005) *Nat Rev Cancer* 5:773–785.
10. Cahill DP, Lengauer C, Yu J, Riggins GJ, Willson JK, Markowitz SD, Kinzler KW, Vogelstein B (1998) *Nature* 392:300–303.
11. Shichiri M, Yoshinaga K, Hisatomi H, Sugihara K, Hirata Y (2002) *Cancer Res* 62:13–17.
12. Shin HJ, Baek KH, Jeon AH, Park MT, Lee SJ, Kang CM, Lee HS, Yoo SH, Chung DH, Sung YC, *et al.* (2003) *Cancer Cell* 4:483–497.
13. Kops GJ, Foltz DR, Cleveland DW (2004) *Proc Natl Acad Sci USA* 101:8699–8704.
14. Weaver BA, Cleveland DW (2005) *Cancer Cell* 8:7–12.
15. Michel LS, Liberal V, Chatterjee A, Kirchwegger R, Pasche B, Gerald W, Dobles M, Sorger PK, Murty VV, Benezra R (2001) *Nature* 409:355–359.
16. Baker DJ, Jeganathan KB, Cameron JD, Thompson M, Juneja S, Kopecka A, Kumar R, Jenkins RB, de Groen PC, Roche P, *et al.* (2004) *Nat Genet* 36:744–749.
17. Meraldi P, Honda R, Nigg EA (2004) *Curr Opin Genet Dev* 14:29–36.
18. Lengauer C, Kinzler KW, Vogelstein B (1998) *Nature* 396:643–649.
19. Mitrou PS, Fischer M, Hubner K (1975) *Acta Haematol* 54:271–279.
20. Grisendi S, Bernardi R, Rossi M, Cheng K, Khandker L, Manova K, Pandolfi PP (2005) *Nature* 437:147–153.
21. Fütterer A, Campanero MR, Leonardo E, Criado LM, Flores JM, Hernandez JM, San Miguel JF, Martínez-A C (2005) *J Clin Invest* 115:2351–2362.
22. Rojas AM, Sanchez-Pulido L, Fütterer A, van Wely KH, Martínez-A C, Valencia A (2005) *FEBS J* 272:3505–3511.
23. Palazzo RE, Vogel JM, Schnackenberg BJ, Hull DR, Wu X (2000) *Curr Top Dev Biol* 49:449–470.
24. Salisbury JL (1995) *Curr Opin Cell Biol* 7:39–45.
25. Lentini L, Iovino F, Amato A, Di Leonardo A (2005) *Cancer Lett* 238:153–160.
26. Wahl AF, Donaldson KL, Fairchild C, Lee FY, Foster SA, Demers GW, Galloway DA (1996) *Nat Med* 2:72–79.
27. Andersen JS, Wilkinson CJ, Mayor T, Mortensen P, Nigg EA, Mann M (2003) *Nature* 426:570–574.
28. Neben K, Giesecke C, Schweizer S, Ho AD, Kramer A (2003) *Blood* 101:289–291.
29. Kearns WG, Yamaguchi H, Young NS, Liu JM (2004) *Genes Chromosomes Cancer* 40:329–333.
30. Giehl M, Fabarius A, Frank O, Hochhaus A, Hafner M, Hehlmann R, Seifarth W (2005) *Leukemia* 19:1192–1197.
31. Hoyt MA, Totis L, Roberts BT (1991) *Cell* 66:507–517.
32. Rieder CL, Maiato H (2004) *Dev Cell* 7:637–651.
33. Li JJ, Li SA (2006) *Pharmacol Ther* 11:974–984.
34. Dai W, Wang Q, Liu T, Swamy M, Fang Y, Xie S, Mahmood R, Yang YM, Xu M, Rao CV (2004) *Cancer Res* 64:440–445.
35. Takahashi T, Haruki N, Nomoto S, Masuda A, Saji S, Osada H (1999) *Oncogene* 18:4295–4300.
36. Hollander MC, Sheikh MS, Bulavin DV, Lundgren K, Augeri-Henmueller L, Shehee R, Molinaro TA, Kim KE, Tolosa E, Ashwell JD, *et al.* (1999) *Nat Genet* 23:176–184.
37. Hollander MC, Philburn RT, Patterson AD, Wyatt MA, Fornace AJ, Jr (2005) *Cell Cycle* 4:704–709.
38. Nigg EA (2002) *Nat Rev Cancer* 2:815–825.
39. Hinchcliffe EH, Miller FJ, Cham M, Khodjakov A, Sluder G (2001) *Science* 291:1547–1550.
40. Kramer A, Mailand N, Lukas C, Syljuasen RG, Wilkinson CJ, Nigg EA, Bartek J, Lukas J (2004) *Nat Cell Biol* 6:884–891.
41. Huang J, Raff JW (1999) *EMBO J* 18:2184–2195.
42. Piel M, Nordberg J, Euteneuer U, Bornens M (2001) *Science* 291:1550–1553.
43. Garcia-Domingo D, Leonardo E, Grandien A, Martínez P, Albar JP, Izpisua-Belmonte JC, Martínez-A C (1999) *Proc Natl Acad Sci USA* 96:7992–7997.